

# Fischer–Tropsch Synthesis with Cu-Co Nanocatalysts Prepared Using Novel Inorganic Precursor Complex

Farzanfar, Javad; Rezvani, Ali Reza\*\*

Department of Chemistry, University of Sistan and Baluchestan, P. O. Box 98135-674, Zahedan, I.R. IRAN

**ABSTRACT:** The structural properties and activities of Cu-Co catalysts used in Fischer-Tropsch synthesis are explored according to their method of preparation. Impregnation, co-precipitation, and a novel method of thermal decomposition were applied to an inorganic precursor complex to generate the Cu-promoted alumina- and silica-supported cobalt catalysts. The precursors and the catalysts obtained by their calcination underwent powder x-ray diffraction, thermal gravimetric analysis, specific surface area measurement using the Brunauer-Emmett-Teller method, scanning electron microscopy, and Fourier Transform InfraRed (FT-IR) spectroscopy. The catalytic performance of all calcined catalysts used in Fischer-Tropsch synthesis was investigated at 280 to 360 °C. The Cu-Co/SiO<sub>2</sub> catalyst was prepared by thermal decomposition of [Cu(H<sub>2</sub>O)<sub>6</sub>][Co(dipic)<sub>2</sub>].2H<sub>2</sub>O/SiO<sub>2</sub>, which served as an optimal precursor for synthesis gas conversion into light olefins. The results highlight the advantages of this novel procedure over impregnation and co-precipitation approaches for effective and durable preparation of cobalt catalysts for Fischer-Tropsch synthesis.

**KEYWORDS:** Fischer-Tropsch synthesis; Preparation method; Novel precursor; Complex; Bimetallic nanocatalyst.

## INTRODUCTION

The conversion of synthesis gas into hydrocarbons or beneficial feedstock for chemicals is called Fischer–Tropsch Synthesis (FTS) and is part of the gas-to-liquid process [1]. Synthesis gas is derived from plentiful natural gas reservoirs. The products produced by FTS are clear of sulfur, nitrogen, and deleterious aromatic materials [2]. It is supposed that a bimetallic catalyst system inclusive of one or two active metal ingredients increases the percentage of light olefins. This means that catalyst composition can have a substantial effect on the molecular weight distribution of the FTS products [3]. The probable electronic interaction between the metal

portions considerably influence the activity and selectivity of the catalysts. Transition metals are normally excellent hydrogenation catalysts, but of the active FTS transient metals, only Co- and Fe-based catalysts have been used in industrial applications [4-5]. Supported cobalt-based FTS catalysts have been investigated because of their good catalytic performance, high-temperature stability, and excellent selectivity to preferred hydrocarbons [6-7].

Active phase dispersion is the function of support, which must demonstrate good mechanical qualities such as resistance to attrition and adequate thermal stability.

---

\* To whom correspondence should be addressed.

+ E-mail: Ali@hamoon.usb.ac.ir

1021-9986/2018/4/15-26

12/\$/6.02

The catalytic activity and product selectivity of Co-catalysts are significantly affected by their physicochemical properties that alter cobalt reducibility and dispersion. The potent interaction of the support and the cobalt precursors results in the formation of highly-dispersed catalysts. Alumina- and silica-supported catalysts are commonly employed in the Fischer–Tropsch reaction because they offer adjustable mechanical and favorable surface properties that correlate with those of the supports [8-10]. Improving the features of the catalyst by adding a secondary metal or metal oxide has been suggested to enhance the catalytic performance of the cobalt FTS catalyst [11].

Together with the support and promoter, the nature of the cobalt precursor and its manner of preparation influence the reducibility and dispersion of the catalyst. A novel approach for the preparation of cobalt particles of the desired size and their deposition onto the support is necessary [12]. Commercial Co-FTS catalysts are generally produced by impregnation of a metal precursor in an aqueous solution in sufficient amounts into porous support (SiO<sub>2</sub>, Al<sub>2</sub>O<sub>3</sub>, or TiO<sub>2</sub>). Studies have prepared supported cobalt-based FTS catalysts by incipient wetness impregnation [9-10], co-precipitation [11, 13], sol-gel [14], fusion [15] and microemulsion [16].

The present study investigated the effect of preparation method and support on the structural properties and catalytic activities of Cu-Co catalysts in High-Temperature Fischer-Tropsch Synthesis (HTFTS). The physicochemical characteristics were investigated using X-Ray Diffraction (XRD), Thermo Gravimetric Analysis (TGA), Brunauer-Emmett-Teller (BET) analysis of the surface area, and Scanning Electron Microscopy (SEM).

The use of inorganic precursor complexes is an ideal approach to the synthesis of materials having two (or more) metallic or oxide phases and provides benefits such as excellent metal interaction, homogeneous dispersion of the metals in each segment of the support, and maximum loading to enhance catalytic performance [17-20].

## EXPERIMENTAL SECTION

### Materials

Reagent-grade Co(NO<sub>3</sub>)<sub>2</sub>.6H<sub>2</sub>O, Cu(NO<sub>3</sub>)<sub>2</sub>.3H<sub>2</sub>O,  $\gamma$ -Al<sub>2</sub>O<sub>3</sub>, SiO<sub>2</sub>, and pyridine-2,6-dicarboxylic acid (dipicolinic acid, H<sub>2</sub>dipic) were purchased from Aldrich and used as received. Based on the relevant literature,

ammonium pyridine-2,6-dicarboxylate (ammonium dipicolinate, (NH<sub>4</sub>)<sub>2</sub>dipic) was prepared by the reaction of ammonia (15 ml) with pyridine-2,6-dicarboxylic acid (1000 mg; 6 mmol) at 75°C. Amorphous SiO<sub>2</sub> with a 200 m<sup>2</sup>/g specific surface area, an average pore diameter of 18-22 nm, and an average pore volume of 1.4-2 cm<sup>3</sup>/g was used in this research. Bare  $\gamma$ -Al<sub>2</sub>O<sub>3</sub> with a 162-m<sup>2</sup>/g specific surface area, the average pore diameter of 10.7 nm, and average pore volume of 0.47 cm<sup>3</sup>/g was employed as catalytic support.

### Preparation of supported Cu-Co catalysts

#### Preparation of [Cu(H<sub>2</sub>O)<sub>6</sub>][Co(dipic)<sub>2</sub>].2H<sub>2</sub>O

Ammonium pyridine-2,6-dicarboxylate (402 mg; 2 mmol) was dissolved in water (20 ml) and added dropwise under continuous stirring to an aqueous solution (5 ml) of Co(NO<sub>3</sub>)<sub>2</sub>.6H<sub>2</sub>O (291 mg; 1 mmol). After 4 h of stirring at room temperature, Cu(NO<sub>3</sub>)<sub>2</sub>.3H<sub>2</sub>O (242 mg; 1 mmol) was added to the solution. The mixture was stirred for 1 h for reaction and then left in the air at room temperature. The dark red crystals that formed in the mixture were collected at a yield of about 60% after 2 wk. Anal. Calcd. for C<sub>14</sub>H<sub>22</sub>CoCuN<sub>2</sub>O<sub>16</sub> (%; 596807 mg): C, 28.17; H, 3.72; N, 4.69. Found: C, 28.08; H, 3.68; N, 4.67%. - IR (KBr):  $\nu = 3401, 3190, 1656, 1621, 1562, 1432, 1384, 1281, 1185, 1083, 775, 726, 688, 594, 484, 433$  cm<sup>-1</sup>. - UV-vis (H<sub>2</sub>O):  $\lambda_{\text{max}} = 221, 227, 267, 578, 773$  nm. -  $A_M$  (H<sub>2</sub>O) = 144 ohm<sup>-1</sup> cm<sup>2</sup> mol<sup>-1</sup>.

#### Preparation of [Cu(H<sub>2</sub>O)<sub>6</sub>][Co(dipic)<sub>2</sub>].2H<sub>2</sub>O/Al<sub>2</sub>O<sub>3</sub> precursor

The [Cu(H<sub>2</sub>O)<sub>6</sub>][Co(dipic)<sub>2</sub>].2H<sub>2</sub>O (10 mmol; 5970 mg) was dissolved in 100 ml distillate water and to this solution was added  $\gamma$ -Al<sub>2</sub>O<sub>3</sub> (1000 mg). To dehydrate the suspension, it was mixed and vaporized at 30°C to dehydration.

#### Preparation of alumina-supported copper-cobalt catalyst, Cu-Co/Al<sub>2</sub>O<sub>3</sub>

The final calcined catalyst was obtained after calcination of the [Cu(H<sub>2</sub>O)<sub>6</sub>][Co(dipic)<sub>2</sub>].2H<sub>2</sub>O/Al<sub>2</sub>O<sub>3</sub> precursor at 800°C for 4 h in an atmosphere of static air in an electric furnace. The final black Cu-Co/Al<sub>2</sub>O<sub>3</sub> catalyst was collected and retained in a desiccator. This sample was labeled as CuCoAlIPC.

#### *Preparation of $[\text{Cu}(\text{H}_2\text{O})_6][\text{Co}(\text{dipic})_2].2\text{H}_2\text{O}/\text{SiO}_2$ precursor*

The  $[\text{Cu}(\text{H}_2\text{O})_6][\text{Co}(\text{dipic})_2].2\text{H}_2\text{O}$  (10 mmol; 5970 mg) was dissolved in 100 ml distillate water and to this solution was added  $\text{SiO}_2$  (1000 mg). The suspension was stirred and vaporized at 30°C to dehydration.

#### *Preparation of silica-supported copper-cobalt catalyst, Cu-Co/SiO<sub>2</sub>*

The ultimate calcined catalyst was obtained after calcination of  $[\text{Cu}(\text{H}_2\text{O})_6][\text{Co}(\text{dipic})_2].2\text{H}_2\text{O}/\text{SiO}_2$  precursor at 800°C for 4 h in an atmosphere of static air in an electric furnace. The final black Cu-Co/SiO<sub>2</sub> catalyst was collected and retained in a desiccator. This sample was labeled as CuCoSiIPC.

#### *Preparation of Cu-Co reference catalysts*

For purposes of comparison, the alumina- and silica-supported Cu-Co reference catalysts were also produced by impregnation and co-precipitation. The co-precipitation method was carried out by mixing aqueous solutions of cobalt nitrate ( $\text{Co}(\text{NO}_3)_2.6\text{H}_2\text{O}$ ) and copper nitrate ( $\text{Cu}(\text{NO}_3)_2.6\text{H}_2\text{O}$ ) (1:1) with the required quantity of support ( $\gamma\text{-Al}_2\text{O}_3$  or  $\text{SiO}_2$ ) and  $\text{Na}_2\text{CO}_3$  at 30°C while keeping a constant pH value by adding an aqueous solution of NaOH dropwise. The resulting precipitate was aged for 6 h. After aging, the suspension was filtered and the filtrate was washed. Following this, the precipitated product was dried at 120°C and calcined at 800°C for 4 h. These samples are labeled as CuCoAlCP and CuCoSiCP, respectively.

Using the impregnation approach, the specified amounts of cobalt nitrate and copper nitrate were dissolved in water and the support was impregnated with them ( $\gamma\text{-Al}_2\text{O}_3$  or  $\text{SiO}_2$ ). The suspension was aged at 30°C for 6 h and was then filtered. After being dried at 120°C overnight, calcination of the precursor was carried out at 800°C for 4 h to produce the final calcined catalyst. These samples were labeled as CuCoAlIM and CuCoSiIM, respectively.

#### *Catalyst characterization*

##### *XRD*

Powder XRD was performed using a FK60-04 diffractometer. The scans were based on a 2 $\theta$  step size of 0.02° and a counting time of 1.0 s with the help of

a  $\text{CuK}_\alpha$  radiation source which was generated at 40 kV and 30 mA. XRD specimens were prepared by compaction into a glass-backed aluminum sample holder. Data collection was done over a 2 $\theta$  range of 5° to 80° and the phases were identified by matching the experimental patterns with the corresponding reference peaks using the JCPDS chemical spectra data bank.

##### *TGA*

Weight change in the catalyst precursors was measured using a TGA-PL (England) under a flow of dry air. The temperature was increased from room temperature to 950°C using a linear programmer in increments of 10°C/min. The sample weight was 5 to 6 mg.

##### *BET measurements*

Measurement of the surface areas was based on BET. The catalyst precursor pore volumes and calcined samples (before and after testing) were measured by  $\text{N}_2$  physisorption using a Quantachrome Nova 4200 apparatus. Degassing of each sample was done under the nitrogen atmosphere at 300°C for 3 h. The samples were evacuated at -196°C for 66 min to obtain the BET surface areas and pore volumes.

##### *SEM*

A Cambridge S-360 scanning electron microscope was used at 15 kV to observe the morphologies of the catalysts and their precursors. The samples were coated with gold/palladium for 80 s at 20 s intervals before measurement to avoid charging of the problems.

##### *Elemental analysis, conductometric, FTIR, UV-Vis, and spectroscopy based on atomic absorption*

Elemental analysis was performed using a Perkin-Elmer 2400 CHNS/O elemental analyzer. Conductivity was measured using a Ciba-Corning Checkmate 90 conductometer. FTIR spectra were recorded as KBr pellets on a Jasco 460 spectrophotometer. UV-vis spectra were obtained on a Jasco 7850 spectrophotometer. Spectroscopy of the metals was performed based on the atomic absorption using a Varian AA50.

##### *Catalytic activity measurements*

HTFTS activity was measured in a fixed bed stainless steel micro-reactor operated at atmospheric pressure (Fig. S1

in supplementary data). The required quantity of meshed catalyst (1000 mg) was held at the center of the reactor using quartz wool. All catalysts were activated (initially reduced) at their natural places under atmospheric pressure and a flowing H<sub>2</sub>-N<sub>2</sub> stream (N<sub>2</sub>/H<sub>2</sub> = 1; each gas flow rate = 30 ml/min) at 350°C for 12 h before exposure to synthesis gas. Afterward, H<sub>2</sub>/CO (1:1) mixture with a pressure of 1 atmosphere (atm) was used instead of N<sub>2</sub>/H<sub>2</sub>. The Fischer-Tropsch reaction under high temperature was conducted from 280 to 360 °C for 8 h at each temperature. A comprehensive description of the reactor system used is presented elsewhere [2, 4]. Conversion of CO and selectivity of the products were considered for evaluation of catalyst activity:

$$\text{CO conversion(\%)} = \quad (I)$$

$$\left\{ \left[ (\text{moles of CO}_{\text{in}}) - (\text{moles of CO}_{\text{out}}) \right] / \text{moles of CO}_{\text{in}} \right\} \times 100$$

$$\text{Product selectivity(\%)} = \quad (II)$$

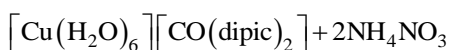
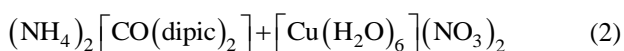
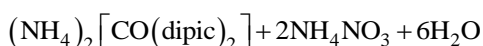
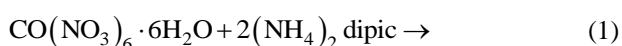
$$\left\{ \text{product mol} / \left[ (\text{moles of CO}_{\text{in}}) - (\text{moles of CO}_{\text{out}}) \right] \right\} \times 100$$

## RESULTS AND DISCUSSION

### Characterization of complexes

#### Description of structure

The molecular ion reaction of [Co(dipic)<sub>2</sub>]<sup>2-</sup> with the complementary units [Cu(H<sub>2</sub>O)<sub>6</sub>]<sup>2+</sup> at room temperature (298 K) led to the formation of heterodinuclear hexa aqua dipicolinate complex [Cu(H<sub>2</sub>O)<sub>6</sub>][Co(dipic)<sub>2</sub>]. The detailed consecutive reactions are condensed in Eqs. (1) and (2) as:



In the suggested structure of the heterodinuclear complex (Scheme S1 in supplementary data) with [Cu(H<sub>2</sub>O)<sub>6</sub>][Co(dipic)<sub>2</sub>].2H<sub>2</sub>O as the divalent anion, [Co(dipic)<sub>2</sub>]<sup>2-</sup> is produced by coordination of two dipicolinate ligands acting as tridentate ligands through their carboxylic oxygen atoms and the nitrogen atoms to Co(II) ions. The charge was balanced by [Cu(H<sub>2</sub>O)<sub>6</sub>]<sup>2+</sup> divalent cations.

### Infrared spectroscopy

The infrared spectrum of the [Cu(H<sub>2</sub>O)<sub>6</sub>][Co(dipic)<sub>2</sub>].2H<sub>2</sub>O complex (Fig. S2 in supplementary data) shows two series of vibrations denoting the aqua and dipicolinate ligands. The broad absorption bands at 3401 and 3190 cm<sup>-1</sup> can be attributed to the asymmetric and symmetric ν(H<sub>2</sub>O) stretching vibrations of the lattice water molecules. Their high intensity and broadness are indicative of intensive H-bonding. The sharp absorption band at 1656 cm<sup>-1</sup> can be attributed to HOH bending vibrations of water molecules in the crystal lattice [21].

In the IR spectrum of the complex, the ν(O-H) vibrations related to the carboxylate group in the dipicolinate ligands are absent, signifying deprotonation of the -COOH group and coordination with Co(II) [22]. Two intense characteristic IR bands accompanied by asymmetric ν<sub>as</sub>(COO) and symmetric ν<sub>s</sub>(COO) stretching vibrations of the dipicolinate carboxylate groups can be observed at 1621 and 1432 cm<sup>-1</sup>, respectively; these shifted after formation of the complex than free dipicolinate ligand. Moreover, the difference in frequency between the symmetric and asymmetric stretching of the dipicolinate carboxylate groups at Δν(COO) = 189 cm<sup>-1</sup> suggests a monodentate mode of carboxylate moiety binding to the Co(II) ions [22-24]. The δ(COO) mode emerges in the spectrum of the free dipicolinate ligand as an intensive band at 701 cm<sup>-1</sup> and shifts to 726 cm<sup>-1</sup>. Three high or medium intensity bands related to the ν(C-O) vibrations of the dipicolinate carboxylate groups can be observed at 1083, 1281, and 1384 cm<sup>-1</sup> [25-26]. The absorption band at 1562 cm<sup>-1</sup> can be attributed to pyridine ring ν(C=C) + ν(C=N) vibration in the dipicolinate ligand. Wagging vibrations of the rings of the pyridine groups can be observed at 688 and 775 cm<sup>-1</sup> [22].

### Electronic and atomic absorption spectroscopy

Atomic absorption spectroscopy analysis revealed acceptable values for Co(II) and Cu(II) ions in the mixed complex, verifying their presence in equimolar amounts of those metals. Analysis of the UV/vis spectrum of this mixed complex attributes copper to the cationic part and cobalt to the anionic part of the compound.

Electronic excitation of the mixed complex (Fig. S3 in supplementary data) in water solution shows several absorption bands in the UV and visible regions.

In the visible region, a distinct absorption band can be seen as a broad maximum at 773 nm in the spectrum of the mixed compound that is caused by d–d transitions of the hexaaquacopper ion. Studies show that the hexaaquacobalt species shows a significant absorption band near 515 nm which is lacking in the mixed compound spectrum, suggesting the absence of this species in the mixed complex. In other words, Co(II) binds to the dipicolinate ligands ( $[\text{Co}(\text{dipic})_2]^{2-}$  moiety and produces a maximum absorption band at about 580 nm and Cu(II) forms the hexaaquacationic moiety [21, 27]. It is believed that the large absorbance in the spectrum below 450 nm is caused by the dipicolinate ligand. In the UV region, three very intense absorption bands at 221, 227, and 267 nm can be seen signifying intra-ligand  $\pi \rightarrow \pi^*$  transitions of the dipicolinate ligand [23].

#### Conductivity measurement

Measurement of the molar conductivity at infinite dilution of the complex ( $\Lambda_M(\text{H}_2\text{O}) = 144 \text{ ohm}^{-1} \text{ cm}^2/\text{mol}$ ) demonstrates that the mixed compound is 1:1 electrolyte in water. This provides structural information and confirms the existence of the cationic  $[\text{Cu}(\text{H}_2\text{O})_6]^{2+}$  and the anionic  $[\text{Co}(\text{dipic})_2]^{2-}$  parts of this complex in aqueous solution [28].

#### Characterization of catalysts and their precursors

##### Infrared spectroscopy

The FTIR spectra of the catalysts prepared by thermal decomposition of the inorganic precursor complex (Figs. S4 and S5 in supplementary data) exhibit characteristic absorption bands of pure alumina and silica. In the spectra of both compounds, the strong, broad OH stretching band appears in the region of  $3420\text{--}3430 \text{ cm}^{-1}$  and the medium intensity H–OH bending peak appears at about  $1637 \text{ cm}^{-1}$ , demonstrating the existence of physically-adsorbed water. On precise examination of the FTIR spectrum of the alumina-supported Cu-Co catalyst, the characteristic bands of absorption identified at about  $1027$ ,  $839$ ,  $721$ ,  $561$ , and  $473 \text{ cm}^{-1}$  (Al–O stretching and bending vibration modes associated with coordinated oxygen around aluminum ions in octahedral and tetrahedral environments) confirm the existence of alumina as the  $\gamma$ -form. In the spectrum of the silica-supported Cu-Co catalyst, the typical absorption bands at about  $1158$  (Si–O–Si network asymmetric stretching

vibrations),  $839$  (symmetric stretching vibrations of Si–O–Si network),  $558$  (bending mode of –OSi–O–) and  $462$  (bending vibration of Si–O bonds)  $\text{cm}^{-1}$  verify the existence of silica. These findings are consistent with FT-IR spectra of alumina- and silica-supported catalysts as reported elsewhere [29–30].

##### XRD

Characterization of Cu-Co catalysts calcined before and after measurement of FTS activity was performed using XRD and are compared with the diffractograms of equivalent fresh calcined and used catalysts in Figs. 1 and 2. The diffraction peaks observed in the Cu-promoted alumina- and silica-supported cobalt catalysts prepared using the three approaches before CO hydrogenation testing (Fig. 1) correspond to  $\text{Co}_3\text{O}_4$  (cubic; JCPDS 00-042-1467), CuO (monoclinic; JCPDS 00-048-1548) and  $\text{Cu}_{0.56}\text{Co}_{2.44}\text{O}_4$  (cubic; JCPDS 01-078-2175) phases.

To allow discrimination of changes in the Cu-Co catalysts prepared by thermal decomposition of the inorganic precursor complex which may have occurred after reduction with the  $\text{H}_2$  stream and throughout the CO hydrogenation reaction, XRD was used to characterize the post-test calcined catalysts and their phases of Co (cubic, JCPDS 00-015-0806),  $\text{Co}_3\text{C}$  (hexagonal; JCPDS 00-043-1144), CoO (monoclinic; JCPDS 01-072-1474) and Cu (cubic; JCPDS 00-004-0836) for the reduced Cu-promoted cobalt catalysts (Fig. 2).

The detectable reflections of these phases were displayed by all samples in each group to a greater or lesser extent. The Cu-Co catalysts display an apparent difference in the ratio between the intensive peaks of both phases at  $36.72$  ( $\text{Cu}_{0.56}\text{Co}_{2.44}\text{O}_4$ ) and  $35.54$  (CuO). It could be deduced that Cu-Co catalysts prepared by thermal decomposition of the inorganic precursor complex (CuCoAlIPC and CuCoSiIPC) contains a higher percentage of non-stoichiometric spinel type  $\text{Cu}_{0.56}\text{Co}_{2.44}\text{O}_4$  than of the CuO oxide phase. In the Cu-Co reference catalysts (CuCoAlCP, CuCoSiCP, CuCoAlIM, and CuCoSiIM), the prevalent phase is CuO. These results suggest that thermal decomposition of inorganic precursor complex promotes chemical interactions between the Cu–Co–O species.

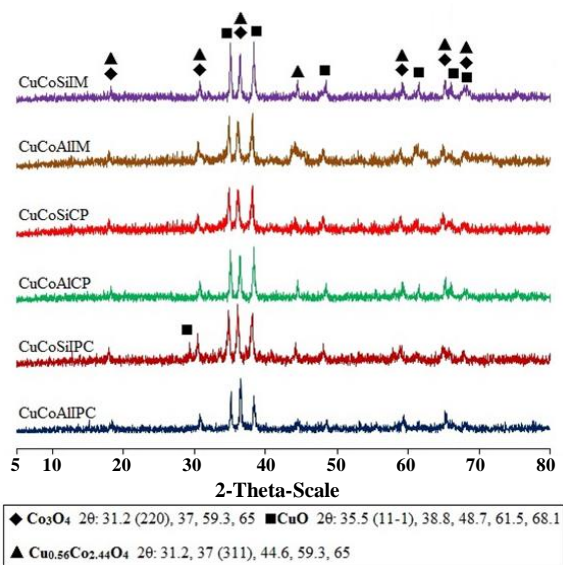
Tables 1 and 2, respectively, present the average sizes of the crystallites calculated for the whole fresh calcined

**Table 1: Structural parameters of fresh calcined Cu-Co catalysts prepared using three different methods.**

Samples	Particle size from XRD (nm)		
	Co <sub>3</sub> O <sub>4</sub>	CuO	Cu <sub>0.56</sub> Co <sub>2.44</sub> O <sub>4</sub>
CuCoAlIPC	30.6	56	31.5
CuCoSiIPC	55	31.2	31.5
CuCoAlCP	30.7	56.1	56.4
CuCoSiCP	114.8	31.4	56.4
CuCoAlIM	36.1	49.3	55.3
CuCoSiIM	64.8	38.6	57.8

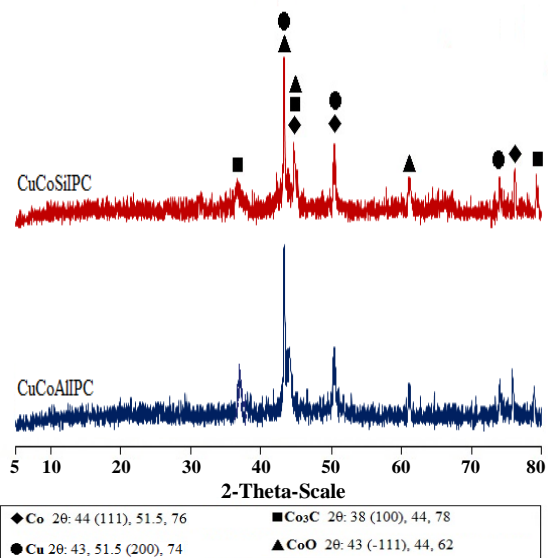
**Table 2: Structural parameters of used calcined Cu-Co catalysts prepared using the thermal decomposition of the inorganic precursor complex method.**

Samples	Particle size from XRD (nm)			
	Co	Co <sub>3</sub> C	CoO	Cu
CuCoAlIPC	48.2	27.4	29.3	34.6
CuCoSiIPC	35.7	15.8	18.2	40.5

**Fig. 1: Powder x-ray diffraction patterns of fresh calcined Cu-Co catalysts prepared by three different procedures before the CO hydrogenation test.**

Cu-Co catalysts and for the used calcined Cu-Co catalysts prepared by thermal decomposition of the inorganic precursor complex using Scherrer's equation.

The full width at half-maximum diffraction peaks selected ((Co (111), Co<sub>3</sub>C (100), CoO (-111), Co<sub>3</sub>O<sub>4</sub> (220), Cu (200), CuO (11-1), and Cu<sub>0.56</sub>Co<sub>2.44</sub>O<sub>4</sub> (311) crystallographic planes) were used to calculate the

**Fig. 2: Powder x-ray diffraction patterns of used calcined Cu-Co catalysts prepared by thermal decomposition of inorganic precursor complex method after the CO hydrogenation test.**

average particle sizes. Narrow diffraction peaks signify large particles and broad diffraction peaks signify small particles. The average particle sizes were the smallest for the alumina-supported Cu-Co catalysts. They were also smaller for the alumina- and silica-supported Cu-Co catalysts prepared by thermal decomposition in comparison with those for the reference Cu-Co catalysts

prepared by impregnation and co-precipitation. These results clearly show that thermal decomposition improved the dispersion of a metal, metal carbide, and metal oxide phases and facilitated generation of smaller particles than those present on the reference samples.

#### TGA-DTG

Characterization of the precursors used for the preparation of the calcined Cu-Co catalysts by the three procedures was performed by TGA under a flow of dry air at 25 to 950 °C at increments of 10°C/min to evaluate the thermal stability and measure weight loss from the increase in sample temperature. Figs. S6-S11 (supplementary data) show the TGA-DTG curves of all precursors and the thermal analytic results are presented in Tables S1-S3 (supplementary data). The general thermal behaviors of the equivalent compounds by preparation method show the same trend.

It can be seen from Tables S1-S3 that thermal decomposition of the Cu-promoted alumina- and silica-supported cobalt precursors prepared by the inorganic precursor complex ( $[\text{Cu}(\text{H}_2\text{O})_6][\text{Co}(\text{dipic})_2].2\text{H}_2\text{O}/\text{support}$  precursors; support =  $\text{Al}_2\text{O}_3$ ,  $\text{SiO}_2$ ) occurred in four steps of weight loss (Figs. S6-S7 in supplementary data). Increasing the temperature, the first and second degradation steps occur between 40 and 150 °C and correspond to the elimination of the two lattices and the six coordinated water molecules, respectively. The dehydrated species are stable up to 300°C. Upon further heating, the last two consecutive steps of weight loss occur and continue up to 500°C. These steps of weight change can be attributed to the decomposition of the two coordinated pyridine-2,6-dicarboxylate ions. The compounds do not lose weight at higher temperatures up to 950°C. The residues are stable oxide phases and the final decomposition products can be recognized by FTIR spectroscopy and XRD.

Thermal decomposition of Cu-promoted alumina- and silica-supported cobalt precursors prepared by impregnation occur at four steps weight loss (Figs. S8-S9 in supplementary data). As the temperature increased, the first and second decomposition steps occur at 50 to 175 °C. These represent the loss of physically-adsorbed water and dehydration from the micropores of the hydroxide gel, respectively. Decomposition of nitrate and dehydroxylation form the final two steps of weight loss at 200 to 550 °C.

The four main thermal effects emerge from the TGA-DTG profile of the Cu-promoted alumina- and silica-supported cobalt precursors prepared by co-precipitation (Figs. S10-S11 in supplementary data). As the temperature increased, the first and second weight loss steps occur between 50 and 145 °C and denote the removal of absorbed water. The last two steps of weight loss occur at 300 to 450 °C for the alumina-supported Co-based precursors and at 600 to 800 °C for the silica-supported Co-based precursors. The decomposition at these temperatures is caused by the degradation of hydroxyl, the basic nitrate precursor, and hydroxy, the basic carbonate precursor.

#### BET measurements

Identification of the catalyst precursors prepared by thermal degradation of the inorganic precursor complex ( $[\text{Cu}(\text{H}_2\text{O})_6][\text{Co}(\text{dipic})_2].2\text{H}_2\text{O}/\text{support}$  precursors; support =  $\text{Al}_2\text{O}_3$ ,  $\text{SiO}_2$ ) and all Cu-Co catalysts calcined (before and after FTS activity) prepared by the three procedures was performed by BET measurement and are shown in Tables 3 and 4.

As shown, the catalyst precursors have much lower specific surface areas and pore volumes than the calcined Cu-Co catalysts. It is clear that calcination induces further changes in the surface areas and pore volumes of the calcined samples. The results also reveal that the calcined Cu-Co catalysts prepared by thermal decomposition have higher BET specific surface areas than the calcined Cu-Co catalysts prepared by impregnation and co-precipitation.

The use of an adequate preparation method (thermal inorganic precursor complex decomposition) increased the BET specific surface areas of these catalysts [31-32], which is evidence of improved dispersion of the active oxide phases and enhancement of catalytic performance of the calcined Cu-Co catalysts. After the Fischer–Tropsch reaction, the texture-based properties of the calcined Cu-Co catalysts changed. The results revealed that the calcined Cu-Co catalysts prepared by thermal decomposition have lower BET specific surface areas and pore volumes than the fresh calcined Cu-Co catalysts. This may be caused by sintering after the Fischer–Tropsch reaction. The BET data on catalyst precursors and all calcined Cu-Co catalysts strongly agree with the SEM results. The finer particles of the calcined Cu-Co

**Table 3: Textural properties of the Cu-Co catalysts prepared by inorganic precursor complex method.**

Samples		BET specific surface area (m <sup>2</sup> /g)	Pore volume (cm <sup>3</sup> /g)
CuCoAlIPC	Precursor	5.2	0.13
	Fresh calcined	139.1	0.48
	Used calcined	102.1	0.42
CuCoSiIPC	Precursor	6.3	0.09
	Fresh calcined	125.8	0.31
	Used calcined	92.5	0.19

**Table 4: Textural properties of the fresh calcined Cu-Co catalysts produced by impregnation and co-precipitation methods.**

Samples	BET specific surface area (m <sup>2</sup> /g)	Pore volume (cm <sup>3</sup> /g)
CuCoAlIM	115.2	1.68
CuCoAlCP	126.8	0.89
CuCoSiIM	89.3	0.17
CuCoSiCP	109.1	0.74

catalysts should have higher specific surface areas and pore volumes than the catalyst precursors.

#### SEM findings

To comprehend the finely-detailed change in morphology during calcination and Fischer–Tropsch synthesis, the catalyst precursors prepared by thermal degradation  $[(\text{Cu}(\text{H}_2\text{O})_6)[\text{Co}(\text{dipic})_2] \cdot 2\text{H}_2\text{O}/\text{support}$  precursors; support =  $\text{Al}_2\text{O}_3$ ,  $\text{SiO}_2$ ) and all Cu-Co catalysts calcined (before and after measurements of FTS) prepared by the three procedures were scrutinized by SEM and micrographs of the different phases are shown in Figs. 3 and 4 and Figs. S12 and S13 (supplementary data).

The results of SEM indicate that the precursors and calcined Cu-Co catalysts have different morphologies and textures. The SEM images of the catalyst precursors are composed of multiform agglomerates with crystalline-shaped particles of dissimilar sizes.

It is evident that calcination at 800°C for 4 h in a static air, atmosphere produces morphological changes in the calcined catalysts. In the calcined Cu-Co catalysts, the agglomerate sizes are smaller than those of the catalyst precursors. The morphologically calcined Cu-Co catalysts prepared by thermal decomposition are different from the calcined Cu-Co catalysts prepared by impregnation and co-precipitation and these calcined

Cu-Co catalysts are composed of smaller particles than the calcined reference Cu-Co catalysts. After the Fischer–Tropsch reaction, a change occurs in the morphological properties of the calcined Cu-Co catalysts. The Cu-Co catalysts prepared by thermal decomposition of inorganic precursor complex form larger multiform particles than the untested Cu-Co catalysts because of sintering and adherence of the small grains to large particles.

#### Effect of reaction temperature on HTFTS activity

The effects of reaction temperature of high-temperature FTS of the calcined Cu-Co catalysts prepared by impregnation, co-precipitation, and thermal decomposition at 280 to 360°C in CO conversion were examined. The product selectivity terms are shown in Figs. 5 and 6 and Figs. S14 and S17 (supplementary data).

It can be observed that the HTFTS activity of the calcined Cu-Co catalysts prepared by the three procedures increased at 280 to 360 °C. The highest conversion of CO (57.4%) was reached at 360°C for CuCoAlIPC catalyst. Methane selectivity of these catalysts increased at 280 to 360 °C and the highest selectivity of methane (34.5%) was reached at 360°C for CuCoSiIM catalyst. The increase in temperature resulted in an increase in catalytic function, probably from the promotion of CO bond dissociation and the presence

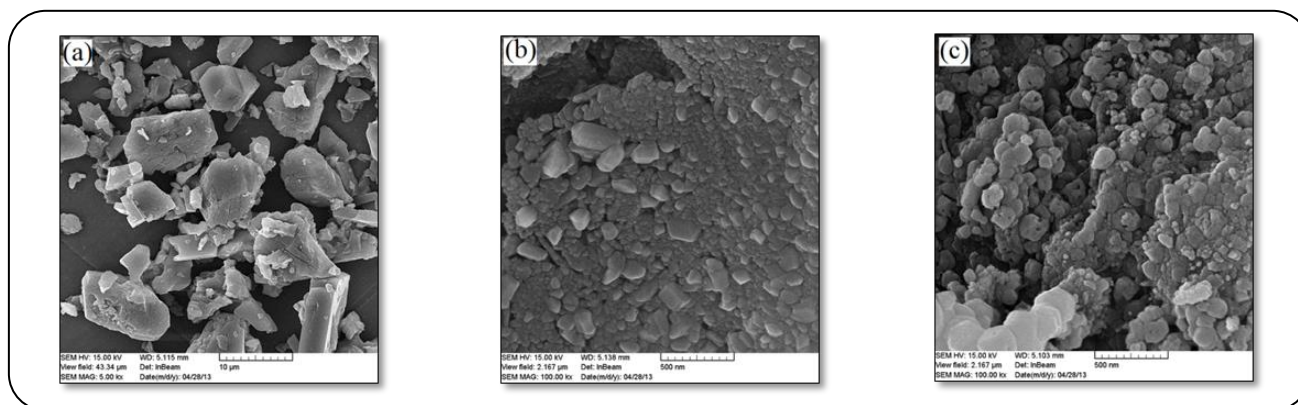


**Fig. 3:** SEM micrographs of Cu-Co/Al<sub>2</sub>O<sub>3</sub> catalyst prepared by thermal decomposition of the inorganic precursor complex a method in (a) precursor, (b) fresh calcined catalyst before the CO hydrogenation test and (c) used a calcined catalyst after the CO hydrogenation test.

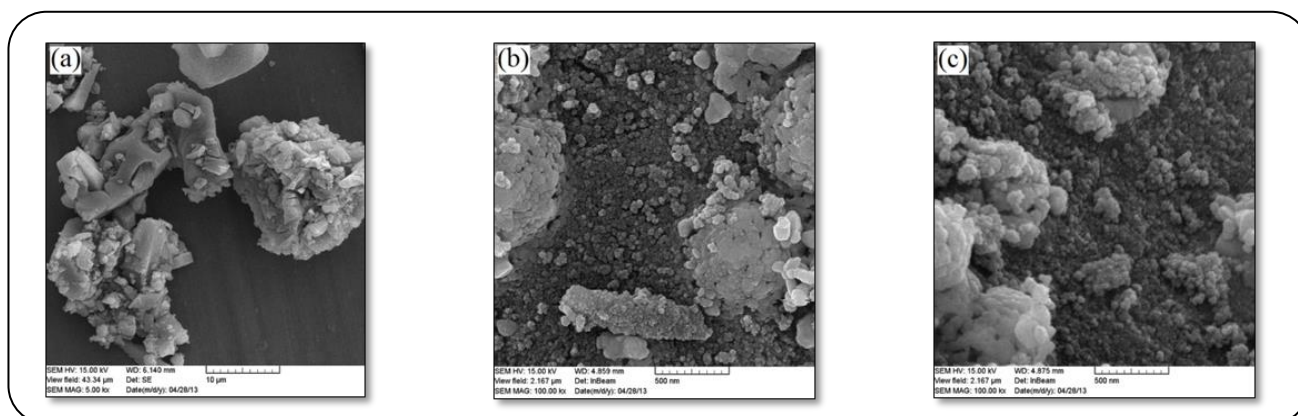


**Fig. 4:** SEM micrographs of Cu-Co/SiO<sub>2</sub> catalyst prepared by thermal decomposition of the inorganic precursor complex method in (a) precursor, (b) fresh calcined catalyst before the CO hydrogenation test and (c) used calcined catalyst after the CO hydrogenation test.

of more surface atoms, which increased the formation of hydrocarbons. An increase in the temperature of reaction provided more surface H atoms to generate large quantities of methane [33].

The results showed that CO conversion and hydrocarbon selectivity notably depend on the method of preparation of the catalysts. The calcined Cu-Co catalysts provided by thermal decomposition of inorganic precursor complex showed higher catalytic activity than that of the reference calcined Cu-Co catalysts prepared by impregnation and co-precipitation.

The results also demonstrate that the optimal temperature of the reaction for all calcined Cu-Co catalysts was 320°C, at which light olefin selectivity was higher than at the other reaction temperatures. At this temperature, methane selectivity is fairly low. The results showed that Cu-Co/SiO<sub>2</sub> catalyst prepared by thermal

decomposition of [Cu(H<sub>2</sub>O)<sub>6</sub>][Co(dipic)<sub>2</sub>].2H<sub>2</sub>O/SiO<sub>2</sub> as a precursor exhibited the best performance in high-temperature Fischer-Tropsch synthesis for gas conversion into light olefins.

The method of catalyst preparation affects catalyst activity. The decrease in crystallite size, the increase in BET specific surface area and the improvement in catalytic performance of calcined Cu-Co catalysts prepared by thermal decomposition were compared with the results from the reference calcined Cu-Co catalysts prepared by impregnation and co-precipitation. The thermal decomposition method has the unique advantages of control of size and its bimetallic composition. Most of the nanoparticles maintain the initial bimetallic composition of the inorganic precursor complex, which increases the efficiency of the inorganic complex as a catalyst precursor.

## CONCLUSIONS

Methods based on thermal decomposition of inorganic precursor complex, impregnation, and co-precipitation produce calcined Cu-Co catalysts with diverse structural features. Analysis was performed on the physicochemical properties of  $[\text{Cu}(\text{H}_2\text{O})_6][\text{Co}(\text{dipic})_2] \cdot 2\text{H}_2\text{O}$  complex,  $[\text{Cu}(\text{H}_2\text{O})_6][\text{Co}(\text{dipic})_2] \cdot 2\text{H}_2\text{O}/\text{support}$  precursors, and Cu-Co/support catalysts (support =  $\text{Al}_2\text{O}_3$ ,  $\text{SiO}_2$ ) using different techniques. XRD, TGA, BET, SEM, and FT-IR spectroscopy proved that calcination generates solid cobalt and copper oxides and carbides and gaseous carbon and nitrogen oxides.

Assessment of the catalytic function in the high-temperature Fischer-Tropsch reaction revealed that thermal decomposition of the inorganic precursor complex is more suitable for preparation of active and stable bimetallic oxide catalysts. This method is an alternative that is favorable for preparing highly-dispersed supported dual catalysts for use in various catalytic processes. Catalytic measurements at 280 to 360 °C confirm the performance of CuCoSiIPC catalyst over that of the other catalysts. It is suggested that the higher activity of this sample compared to other calcined Cu-Co catalysts relates to the smaller particle sizes and higher BET specific surface area and the use of silica support.

## Acknowledgment

The authors are grateful to the University of Sistan and Baluchestan (USB) for financial support.

## Supplementary material

The online version of this article contains supplementary material, which is available to authorized users.

Received: Jun. 27, 2016 ; Accepted : Oct. 16, 2017

## REFERENCES

- [1] Trépanier M., Tavasoli A., Anahid S., K. Dalai A., Deactivation Behavior of Carbon Nanotubes Supported Cobalt Catalysts in Fischer-Tropsch Synthesis, *Iran. J. Chem. Chem. Eng. (IJCCE)*, **30**(1): 37-47 (2011).
- [2] Mirzaei A.A., Shahriari S., Arsalanfar M., Effect of Preparation Conditions on the Catalytic Performance of Co/Ni Catalysts for CO Hydrogenation, *J. Nat. Gas. Sci. Eng.*, **3**(4): 537–546 (2011).
- [3] Feyzi M., Mirzaei A.A., Preparation and Characterization of CoMn/TiO<sub>2</sub> Catalysts for Production of Light Olefins, *Iran. J. Chem. Chem. Eng. (IJCCE)*, **30**(1): 17-28 (2011).
- [4] Zare A., Zare A., Shiva M., Mirzaei A.A., Effect of Calcination and Reaction Conditions on the Catalytic Performance of Co–Ni/Al<sub>2</sub>O<sub>3</sub> Catalyst for CO Hydrogenation, *J. Ind. Eng. Chem.*, **19**(6): 1858–1868 (2013).
- [5] Tavasoli A., Karimi A., Khodadadi A.A., Mortazavi Y., Mousavian M.A., Accelerated Deactivation and Activity Recovery Studies of Ruthenium and Rhenium Promoted Cobalt Catalysts in Fischer-Tropsch Synthesis, *Iran. J. Chem. Chem. Eng. (IJCCE)*, **24**(4): 25-36 (2005).
- [6] Tavasoli A., Anahid S., Nakhaeipour A., Effects of Confinement in Carbon Nanotubes on the Performance and Lifetime of Fischer-Tropsch Iron Nano Catalysts, *Iran. J. Chem. Chem. Eng. (IJCCE)*, **29**(3): 1-12 (2010).
- [7] Tavasoli A., Sadaghiani K., Nakhaeipour A., Ahangari M., Cobalt Loading Effects on the Structure and Activity for Fischer-Tropsch and Water-Gas Shift Reactions of Co/Al<sub>2</sub>O<sub>3</sub> Catalysts, *Iran. J. Chem. Chem. Eng. (IJCCE)*, **26**(1): 9-16 (2007).
- [8] De La Osa A.R., De Lucas A., Romero A., Valverde J.L., Sánchez P., Influence of the Catalytic Support on the Industrial Fischer-Tropsch Synthetic Diesel Production, *Catal. Today*, **176**: 298-302 (2011).
- [9] Ali S., Zabidi N.A.M., Al-Marri M.J., Khader M.M., Effect of the Support on Physicochemical Properties and Catalytic Performance of Cobalt Based Nano-Catalysts in Fischer-Tropsch Reaction, *Mater. Today Commun.*, **10**: 67–71 (2017).
- [10] Vosoughi V., Badoga S., Dalai A.K., Abatzoglou N., Modification of Mesoporous Alumina as a Support for Cobalt-Based Catalyst in Fischer-Tropsch Synthesis, *Fuel Process. Technol.*, **162**: 55–65 (2017).
- [11] Jalama K., Coville N.J., Xiong H., Hildebrandt D., Glasser D., Taylor S., Carley A., Anderson J.A., Hutchings G.J., A Comparison of Au/Co/Al<sub>2</sub>O<sub>3</sub> and Au/Co/SiO<sub>2</sub> Catalysts in the Fischer–Tropsch Reaction, *Appl. Catal. A.*, **395**(1-2): 1–9 (2011).

- [12] Sun Y., Yang G., Zhang L., Sun Z., Fischer-Tropsch Synthesis in a Microchannel Reactor Using Mesoporous Silica Supported Bimetallic Co-Ni Catalyst: Process Optimization and Kinetic Modeling, *Chem. Eng. Process. Process Intensif.*, **119**: 44–61 (2017).
- [13] Mirzaei A.A., Sarani R., Azizi H.R., Vahid S., Oliaei-Torshizi H., Kinetics Modeling of Fischer–Tropsch Synthesis on the Unsupported 4 Fe–Co–Ni (Ternary) Catalyst Prepared Using co-Precipitation Procedure, *Fuel*, **140**: 701–710 (2015).
- [14] Ernst B., Libs S., Chaumette P., Kiennemann A., Preparation and Characterization of Fischer–Tropsch Active Co/SiO<sub>2</sub> Catalysts, *Appl. Catal. A.*, **186**(1-2): 145–168 (1999).
- [15] Feyzi M., Mirzaei A.A., Catalytic behaviors of Co-Mn/TiO<sub>2</sub> Catalysts for Fischer–Tropsch Synthesis, *J. Fuel Chem. Technol.*, **40**(12): 1435–1443 (2012).
- [16] Lögdberg S., Lualdi M., Järås S., Walmsley J.C., Blekkan E.A., Rytter E., Holmen A., On the Selectivity of Cobalt-Based Fischer–Tropsch Catalysts: Evidence for a Common Precursor for Methane and Long-Chain Hydrocarbons, *J. Catal.*, **274**(1): 84–98 (2010).
- [17] Hadadzadeh H., Rezvani A.R., Salehi Rad A.R., Khozaymeh E., A Novel Method for Preparation of Alumina-Supported Rhenium-Cesium Catalyst, Re-Cs/ $\gamma$ -Al<sub>2</sub>O<sub>3</sub>, *Iran. J. Chem. Chem. Eng. (IJCCE)*, **27**(3): 37–43 (2008).
- [18] Farzanfar J., Rezvani A.R., Study of a Mn–Cr/TiO<sub>2</sub> Mixed Oxide Nanocatalyst Prepared via an Inorganic Precursor Complex for High-Temperature Water–Gas Shift Reaction, *C. R. Chimie*, **18**(2): 178–186 (2015).
- [19] Farzanfar J., Rezvani A.R., Inorganic Complex Precursor Route for Preparation of High-Temperature Fischer–Tropsch Synthesis Ni–Co Nanocatalysts, *Res. Chem. Intermed.*, **41**(11): 8975–9001 (2015).
- [20] Ye J., Su H., Bai F., Du Y., Zhang Y., Synthesis, Crystal Structure and Properties of a New Lanthanide-Transitionmetal Carbonyl Cluster, *Appl. Organometal. Chem.*, **23**: 86–90 (2009).
- [21] Tabatabaee M., Kukovec B.M., Kazeroonizadeh M., A Unique Example of a co-Crystal of [Ag(atr)<sub>2</sub>][Cr(dipic)<sub>2</sub>] (dipic = dipicolinate; atr = 3-amino-1H-1,2,4-triazole) and Dinuclear [Cr(H<sub>2</sub>O)(dipic)( $\mu$ -OH)<sub>2</sub>] with Different Coordination environment of Cr(III) ions, *Polyhedron*, **30**: 1114–1119 (2011).
- [22] Saravani H., Ghahfarokhi M.T., Esmaeilzaei M.R., Synthesis and Characterization of Superparamagnetic NiBaO<sub>2</sub> Nano-Oxide Using Novel Precursor Complex [Ba(H<sub>2</sub>O)<sub>8</sub>][Ni(dipic)<sub>2</sub>], *J. Inorg. Organomet. Polym.*, **26**: 660–666 (2016).
- [23] Tabatabaee M., Tahriri M., Tahriri M., Ozawa Y., Neumuller B., Fujioka H., Toriumi K., Preparation, Crystal Structures, Spectroscopic and Thermal Analyses of Two co-Crystals of [M(H<sub>2</sub>O)<sub>6</sub>][M(dipic)<sub>2</sub>] and (atrH)<sub>2</sub>[M(dipic)<sub>2</sub>] (M = Zn, Ni, dipic = dipicolinate; atr = 3-amino-1H-1,2,4-triazole) with Isostructural Crystal Systems., *Polyhedron*, **33**: 336–340 (2012).
- [24] Nakamoto K., "Infrared and Raman Spectra of Inorganic and Coordination Compounds", Wiley-Interscience, New York (1997).
- [25] Shakirova O.G., Lavrenova L.G., Korotaev E.V., Kuratieva N.V., Kolokolov F.A., Burdukov A.B., Structure and Spin Crossover in an Iron (II) Compound with Tris(pyrazol-1-yl)methane and the Complex Eu(dipic)<sub>2</sub>(Hdipic)]<sup>2-</sup> Anion, *J. Struct. Chem.*, **57**: 471–477 (2016).
- [26] Siddiqi Z.A., Khalid M., Shahid M., Kumar S., Sharma P.K., Siddique A., Anjuli, H-bonded Supramolecular Assembly via Proton Transfer: Isolation, X-Ray Crystallographic Characterization and SOD Mimic Activity of [Cu(dipic)<sub>2</sub>]<sub>2</sub>[PA-H]<sub>4</sub>·5H<sub>2</sub>O, *J. Mol. Struct.*, **1033**: 98–103 (2013).
- [27] Kirillova M.V., Kirillov A.M., DaSilva M.F.C.G., Kopylovich M.N., DaSilva J.J.R.F., Pombeiro A.J.L., 3D Hydrogen Bonded Metal–Organic Frameworks Constructed from [M(H<sub>2</sub>O)<sub>6</sub>][M'(dipicolinate)<sub>2</sub>].mH<sub>2</sub>O (M/M' = Zn/Ni or Ni/Ni). Identification of Intercalated Acyclic (H<sub>2</sub>O)<sub>6</sub>/(H<sub>2</sub>O)<sub>10</sub> Clusters, *Inorg. Chim. Acta*, **361**(6): 1728–1737 (2008).
- [28] Devereux M., McCann M., Leon V., McKee V., Ball R.J., Synthesis and Catalytic Activity of Manganese(II) Complexes of Heterocyclic Carboxylic Acids: X-Ray Crystal structures of [Mn(pyr)<sub>2</sub>]<sub>n</sub>, [Mn(dipic)(bipy)<sub>2</sub>].4.5H<sub>2</sub>O and [Mn(chedam)(bipy)].H<sub>2</sub>O, *Polyhedron*, **21**(11): 1063–1071 (2002).
- [29] Renuka N.K., Shijina A.V., Praveen A.K., Mesoporous  $\gamma$ -Alumina Nanoparticles: Synthesis, Characterization and Dye Removal Efficiency, *Mater. Lett.*, **82**: 42–44 (2012).

- [30] Damayanti N.P., Preparation of Superhydrophobic PET Fabric from Al<sub>2</sub>O<sub>3</sub>-SiO<sub>2</sub> Hybrid: Geometrical Approach to Create High Contact Angle Surface from Low Contact Angle Materials, *J. Sol-Gel Sci. Technol.*, **56**(1): 47–52 (2010).
- [31] Savost'yanov A.P., Yakovenko R.E., Narochniy G.B., Sulima S.I., Bakun V.G., Soromotin V.N., Mitchenko S.A., Unexpected Increase in C<sub>5+</sub> Selectivity at Temperature Rise in High Pressure Fischer-Tropsch Synthesis over Co-Al<sub>2</sub>O<sub>3</sub>/SiO<sub>2</sub> Catalyst, *Catal. Commun.*, **99**: 25–29 (2017).
- [32] Sedighi B., Feyzi M., Joshaghani M., Preparation and Characterization of Co-Fe Nano Catalyst for Fischer-Tropsch Synthesis: Optimization Using Response Surface Methodology, *J. Taiwan Inst. Chem. Eng.*, **50**: 108–114 (2015).
- [33] Tian L., Huo C.F., Cao D.B., Yang Y., Xu J., Wu B.S., Xiang H.W., Xu Y.Y., Li Y.W., Effects of Reaction Conditions on Iron-Catalyzed Fischer-Tropsch Synthesis: A Kinetic Monte Carlo Study, *J. Mol. Struct. THEOCHEM*, **941**(1-3): 30–35 (2010).